Experimental study of oil cooling systems for electric motors

Tanguy Davin, Julien Pellé, Souad Harmand, Robert Yu

Applied Thermal Engineering 75 (2015) 1-13

Experimental study of oil cooling systems for electric motors

Tanguy Davin [a, b, c, *], Julien Pellé [a, b], Souad Harmand [a, b], Robert Yu [c]

[a] University of Lille North of France, France
[b] University of Valenciennes, France
[c] Renault, France

Keywords:
Heat transfer
Electric motor
Oil cooling
Experimental bench

A B S T R A C T

The present study focuses on the use of lubricating oil as a coolant for electrical motors. Oil is introduced at each side of a 40 kW test machine to directly cool the stator coil end-windings. An experimental setup has been implemented to test different oil injection patterns. The influence of the oil flow rate, rotation speed and oil temperature has been investigated ($40\ L/h < Qv < 360\ L/h$, $50\ ^\circ C < T_{oil} < 75\ ^\circ C$, $0 < \omega < 4600$ rpm). The results show a strong dependence of the flow rate on global cooling performance, whereas the effect of rotation speed is smaller but can affect local temperature.

1. Introduction

An electrical motor is composed of some elements that can be affected by rising temperature. High electrical currents can generate significant heat loss in the windings. Cooling systems and materials should be optimised to protect these elements. Commonly, windings cannot endure a higher temperature than 180 °C. Furthermore, global efficiency can be affected by the Joule effect. Numerous cooling systems can be found among industry motors. Most systems use air or water as the thermal coolant for simplicity. Most systems cool the motor case or internal space by adding axial air flow using blowing blades and sometimes augmented by rotor channels (Fig. 1).

The former can be implemented as a circulating channel inside the case or by a technique called totally enclosed fan cooling (TEFC): a rotating fan blowing air over the finned carter. Carter cooling implies a long thermal path between the high loss points (i.e., the windings) and the coolant. High heat fluxes must pass through electric insulating components and interfaces formed between parts of the machine. The assembly and impregnation processes might be designed to improve the global conduction but contact resistances remain harmful [1].

During the preliminary phase of this investigation, a nodal model has been developed to represent thermal phenomena inside the machine. After a sensibility study, the major parameters affecting temperature have been identified. Convection on coil end-windings proved to have a great influence, as noted in several previous publications [2,3]. In the latter study, the authors summarise the correlated coefficients on end-winding when air is propelled with a fan. Among numerous studies, Refs. [4,5] present solutions for improving the air convection around the end-windings. A coil winding is a set of electric wire wound around an iron tooth. It comprises natural roughnesses as there are grooves between two wires (Fig. 2).

Because our application is focused on an automotive powertrain (motors of a few dozen centimetres long and wide generating a few dozen kilowatts), the motors are very compact. The range of air convection coefficients might not reach a sufficient level. Due to the presence of lubricating oil in the vicinity of the motor and the heat transfer enhancement that such a liquid provides, oil impingement has been considered. The aim of this article is to investigate on its thermal efficiency but practical difficulties must be considered. Attention must be paid on compatibility between the oil and the machine materials, and aerodynamic losses at high rotation speed level. Also, the oil level should not reach the air gap. This type of cooling might improve compactness but the oil loop might affect the entire cooling structure of the vehicle. In this study, both impinging jets and spray were investigated. The literature provides abundant data for simplified geometries, even for liquids with high Prandtl numbers.

Global [6] and local ([7,8]) studies of laminar jets impinging hot plates can be found in the literature. It appears that a high exchange rate can be obtained, but the Nusselt number sharply decreases as the measurement zone moves away from the impinging zone. Viscosity plays a key role in heat transfer, as shown by Ref. [9]. In

DOI of original article: http://dx.doi.org/10.1016/j.applthermaleng.2014.05.021.

* Corresponding author. Laboratoire TEMPO, Université de Valenciennes et du Hainaut-Cambrésis, Le Mont Houy, 59313 Valenciennes Cedex 9, France.
E-mail address: tanguy.davin@gmail.com (T. Davin).

Nomenclature

A	area (m^2)
D	jet diameter (m)
g	gravity (m/s^2)
Cp	mass-specific heat capacity (J/kg K)
G	thermal conductance (W/K)
I	windings current intensity (A)
l	length scale along windings (m)
L	length (m)
P	power (W)
R	winding electric resistance (Ω)
$Re_d = u \cdot d/\nu$	Reynolds number (−)
T	temperature (°C)
u	mean jet velocity (m/s)
U	voltage across windings (V)
Z	nozzle-to-plate distance (m)
α	temperature coefficient of electrical resistance ($°C^{-1}$)
$\overline{T_{\text{winding}}}$	mean winding temperature (°C)
ε_P	power balance error (−)
ν	kinematic viscosity (m^2/s)
ρ^{elec}	electrical resistivity (Ω m)
ω	rotor speed (rad/s)

Abbreviations

FCN	full cone nozzle
FJN	flat jet nozzle

Subscripts

gl	global
Ref	reference
S	slot
t	tooth
Theo	theoretical
Win	winding
Y	yoke
0	reference for electric resistance definition

this study, several liquids have been tested for impingement. Some authors have tested the influence of roughnesses of the impingement surface on heat transfer. The influence is considerable: the heat flux can be multiplied by 4 with micro-grooves [10] or by 1.8 for special fins [11]. Noteworthy, the impinging zone is kept flat to preserve the high heat transfer in this zone, and the Reynolds numbers tested are high.

Cooling sprays have been investigated by many authors. In Refs. [12], the authors review the literature on the subject. As the temperature must not reach very high values, only the single phase is of interest in the present investigation. Heat transfer increases with the flow rate, which is similar to jet impingement. A local study [13] shows that the high heat transfer zone is extended with a full cone nozzle.

The effect of the surface roughness, in particular straight fins, has been studied by Ref. [14]. The higher is the roughness, the greater is the heat flux. It is explained by the fact that wetted surface is increased and the favourable incidence of the liquid intercepted by the top of the fin. Conduction within the fin and liquid draining might counterbalance these effects. The heat flux might be improved (no quantification for single-phase), particularly for some combination of the nozzle inclination and the fins direction.

A comparison between a jet and a spray array using water has been performed by ([15,16]). It appeared that a spray could provide similar global heat transfer at a substantially lower liquid flow rate.

Nevertheless, real oil flow is quite different from these studies, and only a few studies have shown interest in oil cooling. Locally, the roughnesses on the impinged surfaces are particular due to the winding geometry. Globally, gravity and rotation effects might disrupt the symmetries. The tested global flow rates related to the total surface are also much less important than those of the literature.

2. Experimental setup

2.1. Presentation of the test bench

In the present work, a middle-range power (40 kW), radial flux machine has been used in our experiments. The stator is composed of twelve concentrated windings. The cross section of a winding is 9×25 mm^2 and the end-windings protrude from the iron leaving

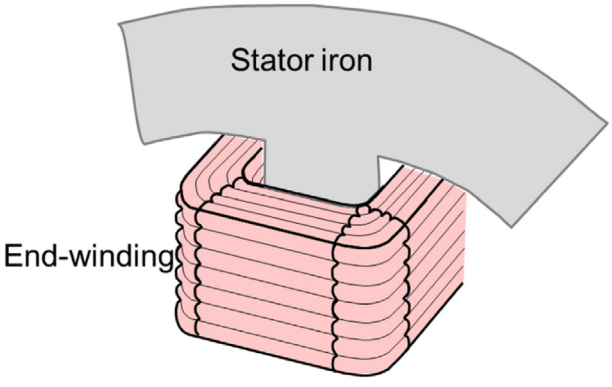

Fig. 2. Sketch of a concentrated end-winding.

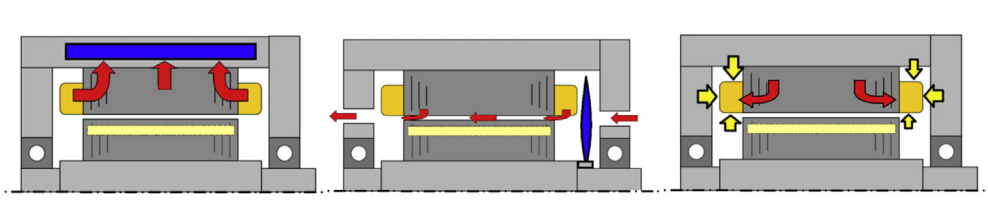

Fig. 1. Cooling strategies with main heat fluxes (red): water jacket, blades on rotor and oil injection on coil end-windings. (For interpretation of the references to colour in this figure legend, the reader is referred to the web version of this article.)

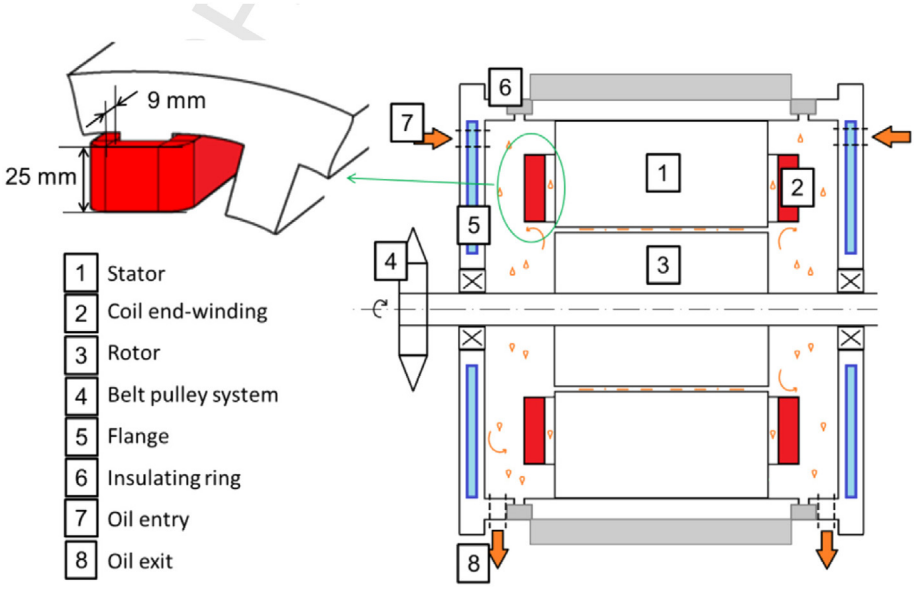

Fig. 3. Experimental machine design.

spaces of 5 mm. The wire windings generate grooves that are theoretically 0.6 mm deep. The space between flanges and stator iron (the side chambers width) is 30 mm. The rotor is composed of eight salient poles covered with end-plates at each side of facing flanges. Thus, the main part of the injected oil must remain in the two side chambers. The air-gap is 1 mm thick. The aim of this paper is to investigate the potential of different cooling configurations on the stator parts. Heat transfer on the rotating parts was not studied.

The purpose of the bench is to enable a general comparison of oil injection methods using visualisation and heat transfer quantification. To truly represent the geometry of the machine, a real stator has been utilised, with a few adaptions for instrumentation purposes. The rotor is entrained by a separate motor with a belt pulley system. To control the power loss inside the machine and limit heat transfer through the rotor, a thermal insulating and non-magnetic material was chosen for the rotor (Fig. 3).

The heat transfer between the flanges and the oil-air mixture as well as between the flanges and the coil end-windings must be studied in detail. As a consequence, flanges have been designed to be thermally separated from the stator as much as possible. Insulating rings were located between these two parts. Additionally, the stator was insulated from ambient air. Cold water ducts have been added inside the flanges to maximise and to quantify the convection heat transfer between the flanges and the oil-air mixture. Hence, the installations contain a water loop for flange cooling, an oil loop and another water loop for oil bath-regulated cooling. Except for the last loop, the temperatures and flow rates were measured precisely (PT100, direct volume measurement). The water flow rate is kept reasonably low to increase the temperature difference between the input and the output. Those loops are described in Fig. 4. A current source is installed to generate constant losses in the windings by the Joule effect.

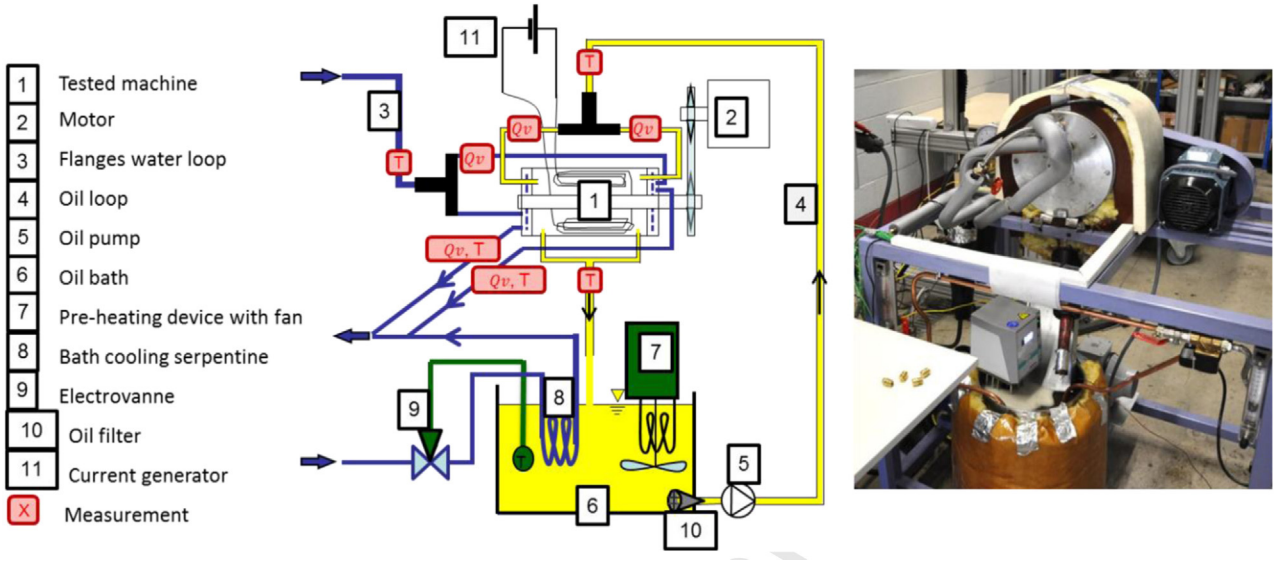

Fig. 4. Description of bench installations (diagram and photograph).

DOI : 10.1016/j.applthermaleng.2014.10.060

Table 1
Summary of the test conditions.

Injection pattern	Full cone nozzle	Flat jet nozzle	Dripping	Multi-jets
Oil flow rate, L/h	40–120	40–130	110–360	150–360
Oil temperature, °C	50–75			
Rotor speed, rpm	0–4600			

When investigating the two-phase flow, the flow, and therefore the heat transfers, will be biased by the entry conditions, the fluid properties and the rotation, thus enabling key parameters to be identified. The entry conditions are defined by the oil injection pattern and the flow rate. The liquid properties might be reduced to the oil temperatures at which viscosity is highly variable (e.g., 30 mm^2/s at 50 °C and 12 mm^2/s at 75 °C). Eventually, the rotating parts in contact with the air and the oil can be described as a flat rotating disc and a rotating cylinder, respective to the rotor side and shaft. Considering the wall velocities, the areas and the vicinity of windings, the rotor disc is assumed to play a key role in heat transfer within the side chambers. The last key parameter is the rotor speed. Parameter ranges are listed in Table 1.

Four oil injection systems (see Fig. 5) have been tested. In all configurations, both sides supply oil in the same manner. Flow rate measurements show a maximum disparity of 5%. First, the mist effect was studied using two spray nozzles. These have been provided by Spraying System Co®. The full cone nozzle (FCN) generates a full cone shape and the flat jet nozzle (FJN) produces a flat jet. Nozzles are referenced by the supplier, such as M8 and HVV04, respectively. The liquid emanating from the nozzles forms a sheet (either a hollow cone or flat jet shape) that breaks into droplets above a certain flow rate. Beyond this critical flow rate, increases result in a reduction of the diameter and densification of droplets. At a given flow rate, a rise in oil temperature, and therefore a diminution in viscosity, will lead to growth in the angle of the sheet. At a given flow rate, the oil sheet is more expanded for a flat jet (angle and length before breakup). The droplet number seems comparable for both nozzles. The flow pattern mainly depends on the flow rate and the oil temperature has slightly less significance. Under experimental conditions, critical flow rates were observed to be approximately 65 L/h at 50 °C and 40 L/h at 75 °C for the two nozzles. Particular attention is needed as given values of the flow rate represent the total rate delivered by the pump. Half of the total rate flows through each nozzle. One nozzle was fixed on the top of the side chamber, directed axially (see Fig. 9). The mist impacts firstly the iron yoke side which is 30 mm far from the injection point.

The second type of injection has been designed to supply oil around coil end-windings in the simplest way possible. Five injection points are located above the five upper end-windings so that, under gravity, all end-windings are likely to be affected. The purpose of this injector is to produce low impact velocities and a correct oil distribution throughout the operating flow range. The orifices are 2.8 mm in diameter and placed very close to the windings surface (ratio $z/d \sim 1$).

Eventually, another injector has been conceived to achieve better efficiency at distributing oil on all twelve end-windings with higher impact velocities. The injector includes three orifices in front of each end-winding, producing jets that impinge on different

Fig. 5. Oil flow pattern for the flat jet nozzle (FJN) and the full cone nozzle (FCN) for low (top: 51 L/h) and high (bottom: 102 L/h) flow rates at 50 °C.

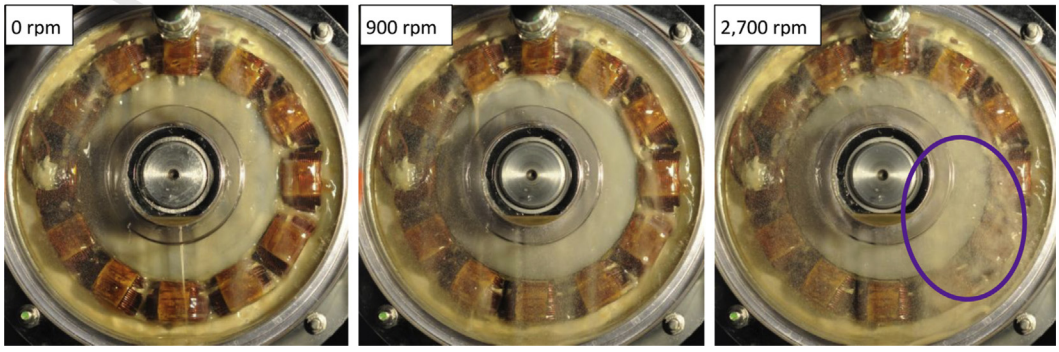

Fig. 6. Photographs of the flat jet nozzle injection (80 °C oil, 130 L/h).

surfaces of the windings: one facing the flange, one facing the carter and one facing the stator tooth. The injector includes 36 orifices of 0.5 mm diameter. The windings roughnesses are then of same value than the jet diameter. The injector produces a multi-jet pattern with a maximum velocity of 7 m/s, which is moderate due to the fragility of the conductors. The orifices are located further from the impingement surfaces (ratio $z/d \sim 12$). For the dripping and multi-jets injectors, in all configurations, jets are laminar ($Re_d < 460$).

Injectors differ from each other by the oil pattern and flow rate range. The means for the generation of the pattern are also different as mist nozzles require relatively high pressure level (until 5 bars for these tests) while the dripping injectors generate negligible pressure loss. Multi-jets represent an intermediate need for the pump pressure. These injectors, despite their different flow rate ranges, have been chosen to compare the effect of changing the position and the pattern of the oil injection on windings dissipation power.

2.2. Measurements and uncertainties

The instrument includes 17 thermocouples attached to different walls. Thermocouples are primarily located on the stator parts. Going forward, measured temperatures at the core of the machine are presented. Four PT100 probes are immersed in water or oil to improve the accuracy of the powers calculation. Flow rate measurements have been achieved to ensure that the distribution between both sides of the machine is correct. A measuring cylinder and a chronometer were used to obtain flow rate values for oil and water. In theory, the machine as a thermal system verifies the power balance:

$$P^{\text{theo}}_{\text{winding}} + P^{\text{theo}}_{\text{friction}} + P^{\text{theo}}_{\text{oil}} + P^{\text{theo}}_{\text{water}} + P^{\text{theo}}_{\text{air}} = 0$$

This equation let appear the winding power, dissipated into windings by the Joule effect, and the friction loss. Both are always positive. The other powers are those dissipated into oil, water and air. The powers dissipated into oil and water are calculated from the measured flow rates and the difference temperature between the input and the output.

For all measurements, the power balance has been achieved to calculate the measurement power balance errorε_P, defined as:

$$\varepsilon_P = \frac{\left|P_{\text{winding}} + P_{\text{friction}} + P_{\text{oil}} + P_{\text{water}} + P_{\text{air}}\right|}{P_{\text{winding}} + P_{\text{friction}}}$$

For the reference configuration with air, P_{windings} has a small value, hence high ε_P values were obtained (a 7% mean and a 22% maximum). Fortunately, the error is highly reduced when operating with oil (a 3% mean and a 7% maximum). A mean uncertainty of 4% and 2% on the flow rate measurements is reached for oil and water, respectively. The uncertainty on the rotor speed is reduced to 2%. During calibration, temperatures measured by thermocouples were not scattered more than 0.3 °C. Maximal difference between PT100 temperatures did not exceed 0.15 °C, which was verified for 0 °C and 100 °C ambience. The next table presents the general uncertainties of the presented thermal power. Interestingly, the friction power component is mostly dissipated by the flange water.

During experiments, voltage and current measurements are of interest to determine the mean temperature of the winding. Indeed, all of the windings put together in series constitute an electrical resistance. As electrical resistivity is a function of the local

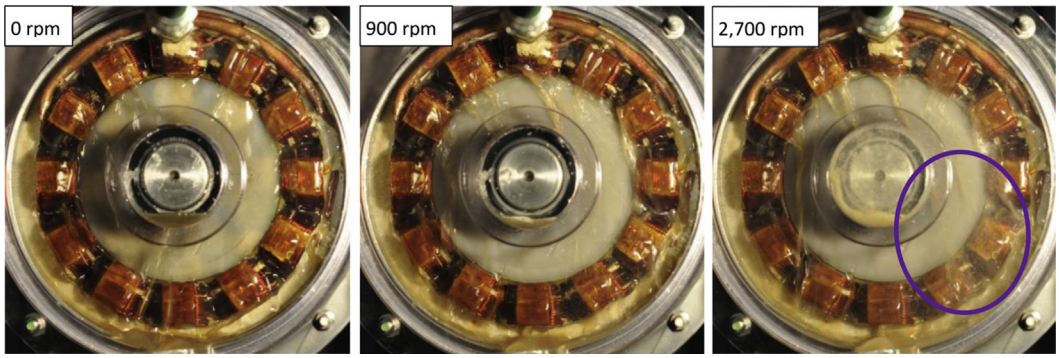

Fig. 7. Photographs of the dripping injection (80 °C oil, 350 L/h).

temperature and the winding cross section is constant, the electric resistance can be described as an affine function of the mean winding temperature:

$$R = \int_0^{L_{\text{winding}}} \frac{\rho_0^{\text{elec}}\left[1+\alpha\left(T_{\text{winding}}(l)-T_0\right)\right]}{A_{\text{winding}}}\mathrm{d}l$$
$$= R_0(T_0)\left[1+\alpha\left(\overline{T_{\text{winding}}}-T_0\right)\right]$$

where $R = U/I$.

In the present study, measurements lead to $\alpha = 0.0040\ ^\circ\text{C}^{-1}$ for $T_0 = 20\ ^\circ\text{C}$. Commonly, an α value of 0.0038 for copper is reported. Because this factor is relatively small, the mean winding temperature accuracy reaches 2 °C. It is important to notice the difference between this temperature and the local temperatures measured by thermocouples. This mean temperature shows the general trend in the winding temperature.

2.3. Flow visualisations

To interpret thermal measurements, visualisations of the motor side flow are provided. A transparent flange has been designed to permit flow observations. A laser sheet was sometimes added to better distinguish drops and droplets. Photographs have been taken for three injection types: mist, dripping and multi-jets. For the first two types, photographs are presented (Figs. 6 & 7) for a clockwise rotation (the negative direction) and an oil temperature of 80 °C at the relative maximum oil flow rate. The multi-jets injection photographs are not included as the injector was hiding a part of the view and the effects of parameter (particularly rotation speed) are less clear than for other two types of injection.

Regarding the nozzle and multi-jets injection, the areas where the moderate velocity impacts seem effective are restricted. The general flow seems to be dominated by falling film and dripping oil for almost all configurations observed, although drops and droplet dispersion seems to be of more importance when using the spray nozzle. In the common flow, a liquid film of variable thickness is formed on the end-winding walls. All of the oil impacted on a winding is concentrated at its lowest point by gravity. Every end-winding corresponds to a substantially null velocity jet emanating from this lowest point. Depending on the amount of oil that is provided on the end-winding, the jet may be continuous or drop-by-drop. The oil flow is schematized on Fig. 8. To identify the windings location, the analogy of a clock dial is considered, as shown on Fig. 9.

The jet streaming from an end-winding may fall either on another end-winding located just below (windings 2, 3, 4, 8, 9, 10), on the housing/yoke (5, 6, 7) or on the rotor side (11, 12 and 1, rarely 2 and 10). Therefore, only the three upper end-windings are likely to form a jet on the rotating part, which then redirects the oil. It is noteworthy that, depending on the flow rate and the rotor speed, jets from windings 2 and 10 might be broken up. In all three configurations that were tested, the three upper windings are supplied with oil. From those visualisations and assuming a correct distribution, the proportion of oil from the total flow rate that is likely to meet the rotating parts is:

- A significant amount for the flat jet nozzle (depending on speed and angle of the oil jet, i.e., drops and droplets dispersion)
- 60% (3 out of 5 jets supplied) for the dripping injector
- 25% (9 out of 36 jets supplied) for the multi-jets injector

Thus, even though total flow rates are smaller for mist nozzles, oil dispersion can be improved because the generation of droplets and the rotation are apparently more efficient.

Attention is then focused on the flow pattern produced when the upper windings jets meet the side rotor disk (Fig. 8). At null speed, the jets adhere to the side wall of the rotor. When the rotation is activated but has a small value, the oil streams over the rotor but is directed toward the right side (the direction of the rotation). So flow rate on this side seems to increase while the flow rate is reduced on the other side. For more than approximately 600 rpm, the jets are split into drops or droplets that mostly impinge on the right-lower quadrant. The higher the rotation speed, the more projections that are observed, especially in this lower-right quadrant. For high rotation speeds, projections on the upper windings nevertheless remain insubstantial. Although conditions are constant during these tests, the flow is unsteady due to random jet and drop breakups by the rotor.

Interestingly, the flat jet is positioned horizontally above the winding 12, only impinging on the flat stator yoke. Even at the highest flow rate, jets are laminar at the orifice output (multi-jets) and impingements do not generate droplet ribbons.

2.4. Thermal measurements

All trials were conducted at a thermal steady state. Prior to any measurement, all operating parameters were set to the desired

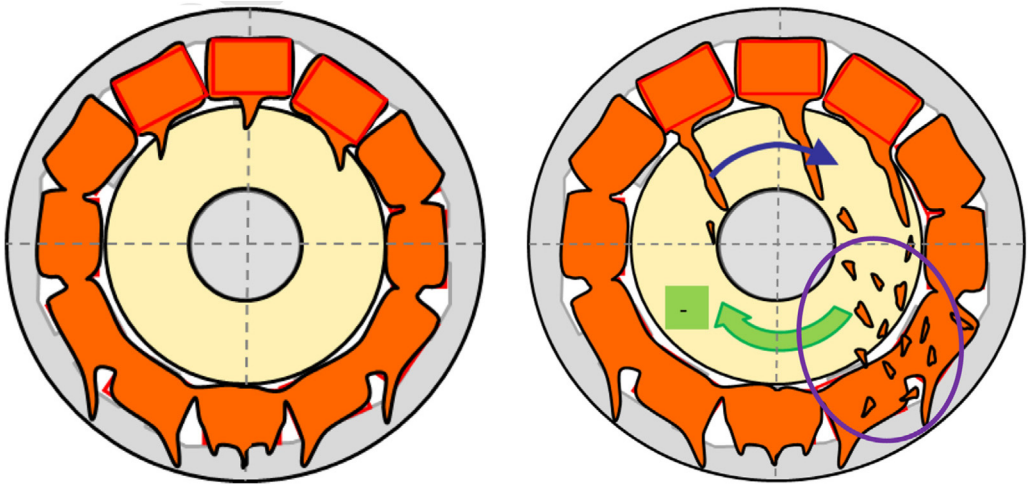

Fig. 8. Sketch of the flow observations at null or low rotation speed (left) and at higher rotation speed (right).

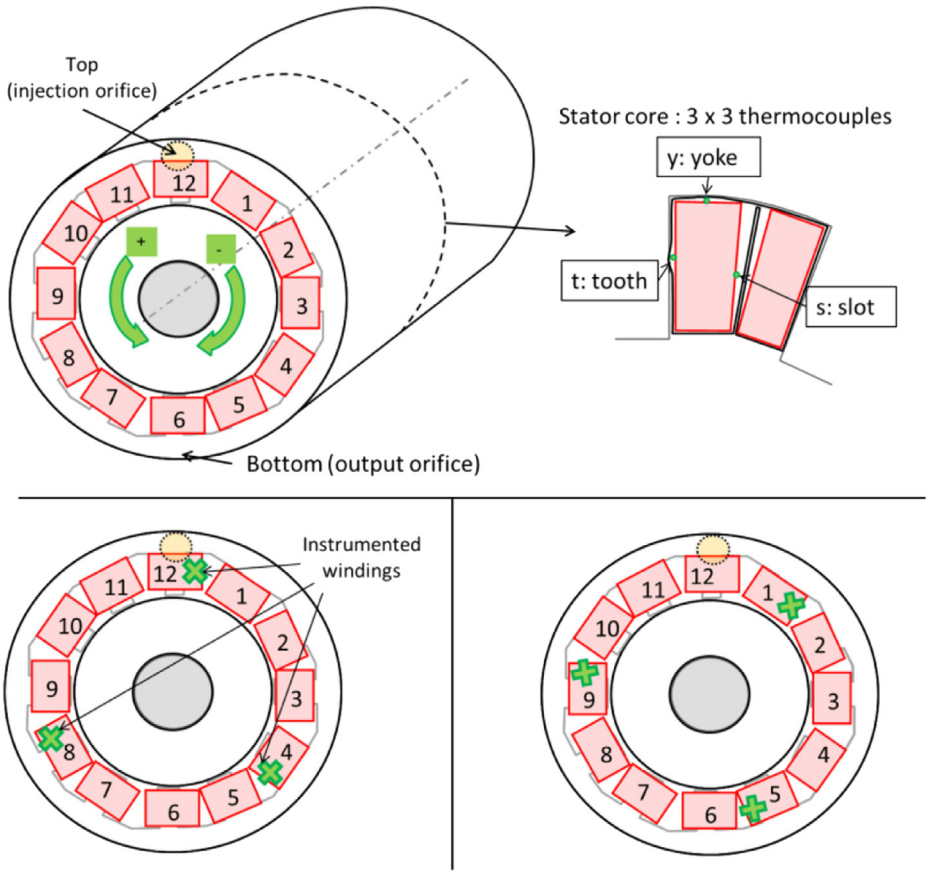

Fig. 9. Instrumented windings locations: winding thermocouple locations in the slot (top), mist and dripping configurations (bottom left) and multi-jets (bottom right).

configurations in terms of the rotor speed, oil temperature and flow rate. The water flow rate was occasionally measured and appeared to be steady. Next, the windings were supplied with current until reaching a general steady state. Thermal measurements were then processed: 10 values were picked up every 30 s. Disparity and variations were checked. Resulting averaged values were taken into account. The winding power appeared to be stable; only one measurement of U and I was taken.

The mean winding temperature was maintained at a constant temperature for the purpose of comparison. The power supplied to the windings is the key parameter that denotes the global efficiency of the injection under special conditions. Attention must be paid, however, as this power does not correspond to the dissipation capability of a real machine. This power mainly reflects the heat transfer efficiency on side stator parts as it is insulated from the flange. The winding power is mostly dissipated in the oil, but about half of this power is transmitted to the water before exiting (see Table 2). Flange water cooling might thus play a larger than negligible role in the heat transfer.

Two oil input temperatures were tested, 50 and 75 °C. It is noteworthy that the mean winding temperature was set to approximately 90 °C during mist tests for a 50 °C oil temperature.

Table 2
Mean power values and measurement uncertainties.

Power	$P_{winding}$	$P_{friction}$	P_{oil}	P_{water}	P_{air}
Mean value, W	700	90	−350	−410	−30
Mean uncertainty	2%	12%	22%	7%	–

The rest of the measurements were conducted at a 110 °C winding temperature.

Some temperature variations might be mentioned during a few tests, in particular for some lower windings. These variations were up to 7 °C at the core of the machine, where fluctuations must be smoothed. The variations can be logically linked to the unsteady flow due to breakups of the jets. As variations were observed for only a few tests, the phenomenon was not investigated.

2.4.1. *Reference configuration: air cooling*

First, measurements have been achieved for a reference case without any oil injection. The winding dissipation power is divided

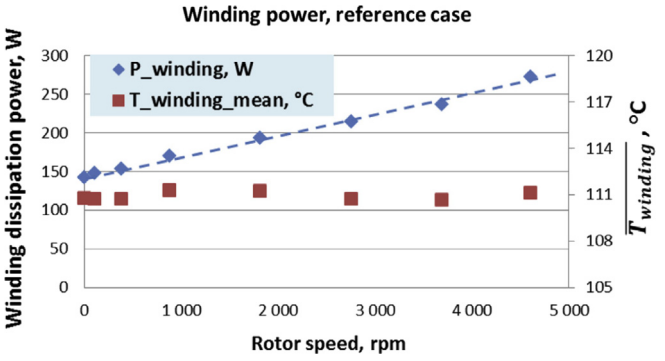

Fig. 10. Reference configuration (air only): rotor speed influence on power dissipation.

between ambient air dissipation and water dissipation, i.e., conduction through insulating rings and inside air convection. The latter thermal path comprises transfer from the side of the stator – particularly the end-windings – to the inside air then from the inside air to the water-cooled flanges. Water, ambient air and carter temperatures remained quasi-constant during measurements so that only the inside air convection power is influenced by the rotor speed. Approximately 30 W are dissipated by ambient air and 20 W for each side by the water through the insulating rings. Within a constant range (approximately 70 W), the winding dissipation power plotted in Fig. 10 accurately reflects the heat transfer by the inside air convection. It is interesting to observe that the inside convective transfer constantly increases with the rotor speed: 70 W for natural convection and up to 200 W at ω^{max}, corresponding to the 140–270 W range of $P_{windings}$. In this type of motors, electromagnetic losses may reach more than 2000 W. That support the need for a better cooling system; the injection of oil, even a restricted amount, is thus considered.

The literature ([17,18]) provides descriptions of the flow in the case of a shrouded discoid rotor–stator system. Air is tangentially entrained by the rotating disc due to its viscosity. As a result, air is driven centrifugally at the rotor side and centripetally close to the

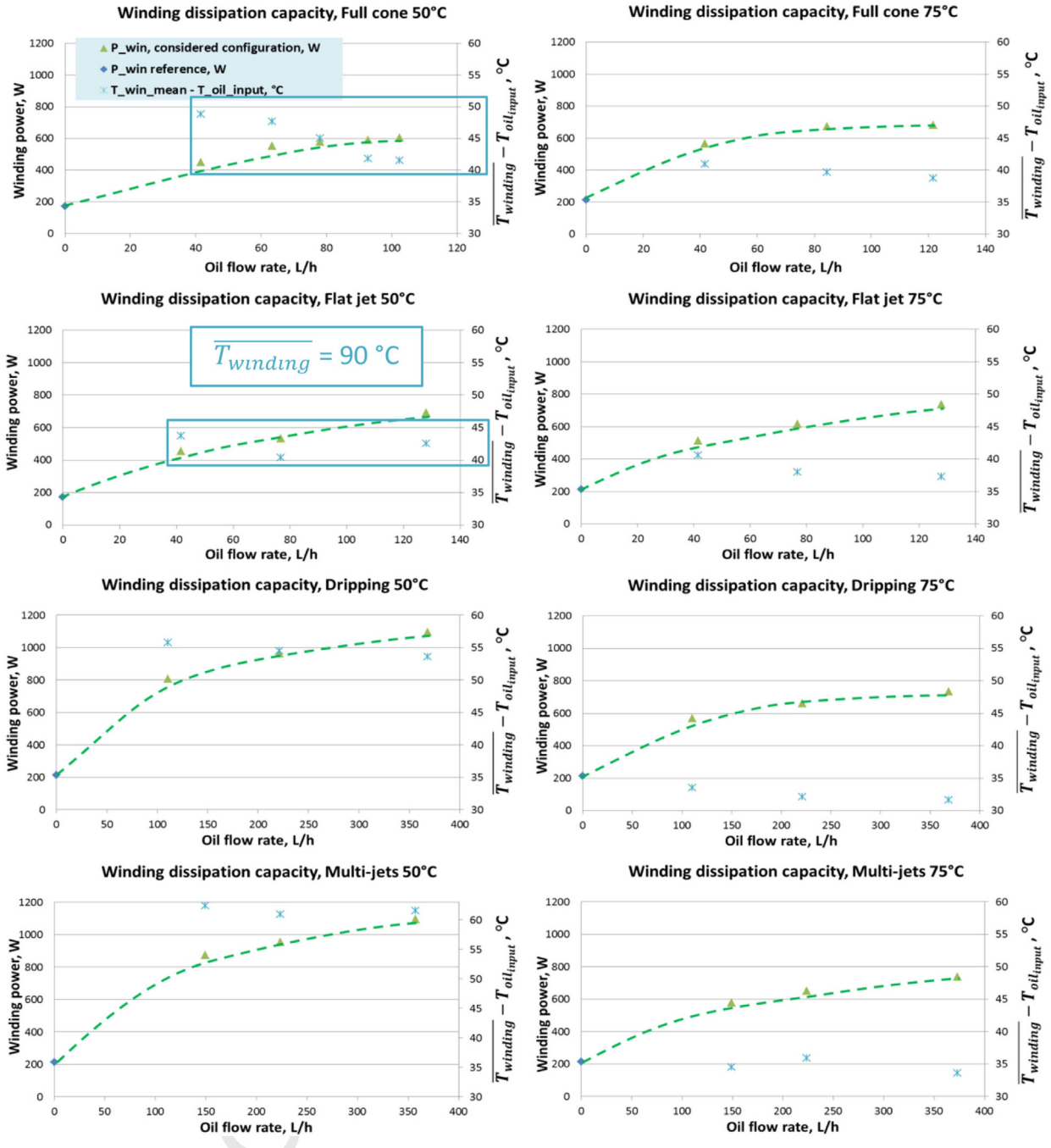

Fig. 11. Influence of oil flow rate and temperature on the winding dissipation power for all injectors (rotor speed = 2750 rpm).

flange. This generates air jets on the stator parts. Considering the two-disc spacing in our study ($e/R_{rotor} = 0.48$), the presence of the flange might not affect the boundary layer over the rotating plate, although the end-windings might. The flow around the end-windings and the stator yoke can then be approximated by an impinging flat jet whose velocity corresponds to the outer radius velocity over a freely rotating disc.

2.5. Global oil cooling

Heat transfer by activate oil injection is investigated in this part. For a better rationalisation, data for air cooling are also displayed on graphs when the comparison is relevant, referred as dark blue points. These data represent measurements for the same parameterisation (mean winding temperature and rotor speed) but without the oil. Air cooling is mentioned as the reference.

2.5.1. Influence of oil flow rate and temperature

As operating points are numerous, the effect of each parameter is processed one at a time. Data are presented in Fig. 11 in the oil flow rate range of each injector at a fixed rotor speed (2750 rpm). Like the reference configuration, the global efficiency is represented by the power dissipated in the windings. The value of the difference between the mean winding temperature and the input oil temperature ($\Delta T = \overline{T_{winding}} - T_{oil_{input}}$) is also shown because it represents the variations of the entry conditions. It is intended to be constant for a dataset. Trend lines are added, taking into account the influence of these small variations on the results. Indeed, if this ΔT is higher when compared to the reference test, the resulting winding power is more substantial than it should be.

All graphs clearly show that an increase in the oil flow rate improves winding cooling, regardless of the injection mean. As expected, the dissipation power is better when oil is injected than in the reference configuration when only air is inside the motor. Data are here presented only for a given rotor speed, but the influence of flow rate on global cooling is noticeable at any rotor speed (even the null speed).

It is noteworthy that for both mist nozzles, datasets for 50 °C oil have been achieved for an approximate mean winding temperature of 90 °C (see red-framed data). That explains why dissipated power is slightly lower than for the input oil temperature of 75 °C. It also accounts for the lower value of the reference dissipation windings. For dripping and multi-jets configurations, the effect of oil temperature is important. For 50 °C oil, the difference $\overline{T_{winding}} - T_{oil_{input}}$ is largely increased and the dissipated power is augmented despite a near tripling of the oil viscosity.

Due to the variation of the tests conditions, the global winding dissipation can be related to the temperature difference between the winding and the oil. A global conductance can be defined in the equation below. Keeping in mind that the total power evacuated by oil is directly linked to ΔT, the oil cooling efficiency of the different injection types can be compared using the global conductance.

$$G_{gl} = \frac{P_{winding}}{\overline{T_{winding}} - T_{oil_{input}}} = \frac{P_{winding}}{\Delta T}$$

Fig. 12 shows a clear comparison of the injection types for similar conditions (winding and oil temperatures). The reference case cannot be included. Global power dissipation capacity is of a comparable level for all injectors within the flow rate overlapping range, approximately 120 L/h. However, it can be observed that the slope of the power lines is steeper for mist generation than for the other injection types. This slope may be due to the significant densification of droplets with increased flow rate because the pressure sharply increases.

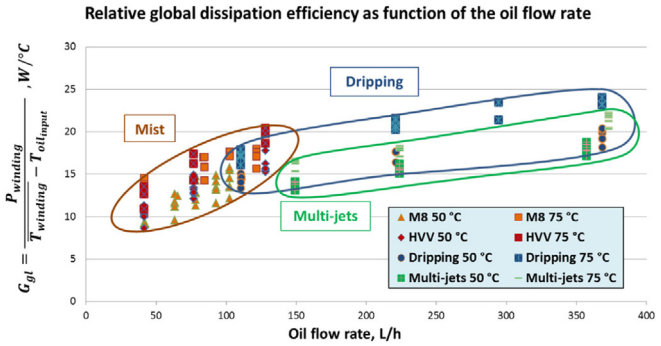

Fig. 12. Relative global oil cooling efficiency depending on the flow rate, for all datasets.

The comparison of the last two injections is interesting. Although the dripping solution only includes a few injection points compared to the multi-jets solution, the global dissipation capacity seems to be slightly surpassing. As the entire part of the oil is injected in the upper region, a higher flow rate is assumed to reach all end-windings. The general flow is assumed to be governed by falling film effects. Higher flow rates on the end-windings would thus explain the general trend that the dripping efficiency exceeds that of the multi-jets.

Because data are here given for several rotor speeds, the points scattering render the influence of the rotor speed on the global convective transfer. It can be noticed that this influence seem relatively strong for the mist injection while quite negligible for the other two injection types. Relative dissipation is more important at higher oil temperature, which is linked to the decreased viscosity. However, these effects do not counterbalance the temperature difference between winding and oil as absolute global dissipation is lower at a higher oil temperature.

2.5.2. Influence of rotor speed

For each injection type, Fig. 13 shows data for varying rotor speed at a given flow rate. This flow rate corresponds to the maximum test flow rate because it seems close to the applied operating conditions relative to each injection type. The results presented were obtained for 120 L/h and 350 L/h for the mist injectors and the last two injectors, respectively. Only 75 °C input oil tests are displayed because the influence of rotor speed on global stator heat transfer is less important than the oil flow rate.

For all injection types, winding power is augmented when rotation is activated. However, this transfer improvement is noticeable for mist, but moderate for dripping and multi-jets. For mist injection, drops and droplets circulation must be promoted by rotation at a small rotation speed. Nevertheless, the heat transfer is not increased when the rotation is augmented. Worse still, it is observed to decrease for higher speeds. For the dripping and multi-jets configurations, except at the null rotor speed, the winding power appears to be a constant function of the rotor speed.

Regarding the flow observations, the falling film and dripping effects seem to predominate for all types of injection (except the mist because of the droplets that are generated). The data report measurements for the maximum flow rates. This means that the mist is denser and the droplet influence is assumed to be greater. It also implies that the influence of rotation on global falling film and dripping transfer is negligible, which is not the case for droplets. This result is logical as the droplet's inertia is much smaller than the drop's inertia. While rotational effects constantly improve heat transfer when only air is present inside the machine, oil cooling comes to a saturation point above a low speed. Non-uniform

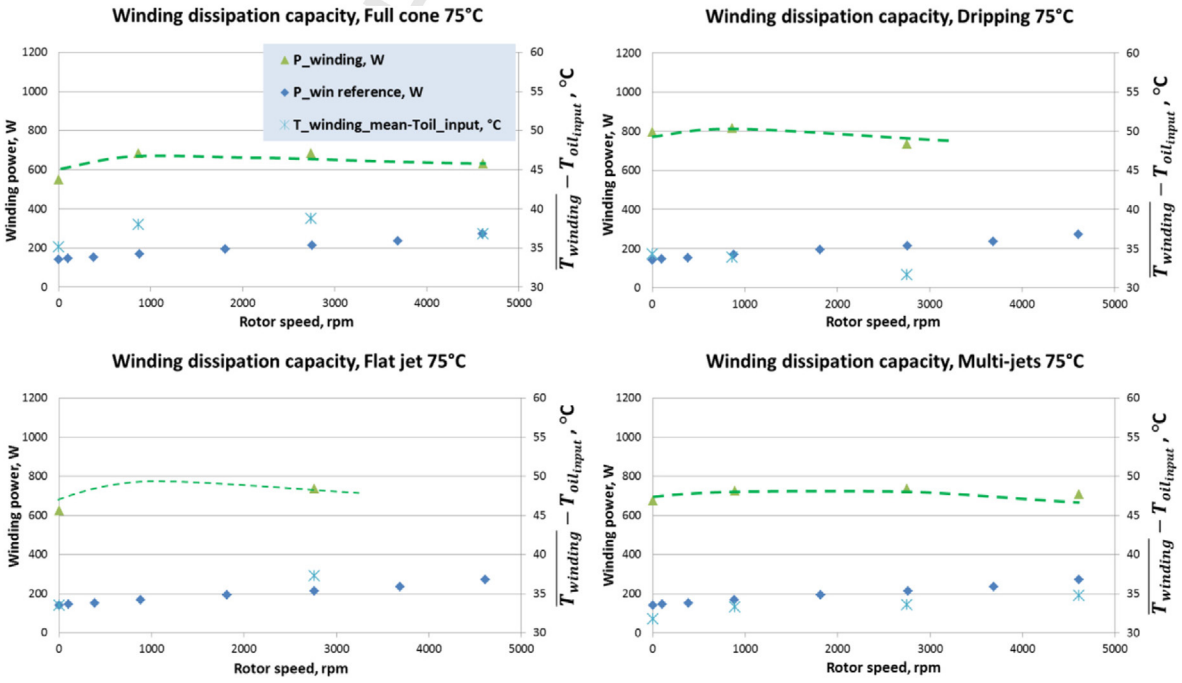

Fig. 13. Influence of rotor speed on winding power for the relative maximum oil flow rate.

repartition of droplets might explain this global saturating efficiency.

A further investigation is needed to interpret the impact of rotation, particularly for mist generators. That is why the local temperature analysis was performed and presented.

2.6. Local oil cooling

In this part of the study, local temperatures are investigated. First, a few phenomenon of inside stator conduction are mentioned. A winding is a body of varnish-coated copper assembled with resin. Air is also likely to be confined inside. A winding is then thermally anisotropic. Its equivalent radial conductivity is far smaller than its axial conductivity. Because of these properties and the restricted heat generation, temperature gradients inside the windings can be very substantial, especially radially. By cooling the end-windings in the same manner for both sides, local hotspots are located at the core of the machine (median plane).

By means of thermocouples located around radial positions, disparities can be identified. For these reasons, thermocouples were implanted on three different windings and each comprises three measurement points on the winding surface. A diagram of the thermocouple locations is provided in Fig. 9. It is noteworthy that the stator radial position has been changed for the multi-jets test series. For these measurements, one thermocouple was faulty.

Though these thermocouples are located in the highest temperature section of the windings, temperature measurements are likely to be of a smaller value than the maximum winding temperature. This point is actually to be found closer to the centre of the cross section due to the heat loss diffusion.

In the following graphs, direct temperature measurements are indicated. For comparison convenience, mean windings temperatures are added. Only the 75 °C oil data are provided. The effects of the rotation speed and the oil flow rate on the temperature along the radial position are discussed. Black arrows are affixed to better show the general trend of the parameter effects. A strong dependence on a parameter would imply a clear demarcation from the mean winding temperature trend.

2.6.1. Impact of rotation on local temperatures

The impact of rotation speed is further studied. The data displayed in Fig. 14 are at a given mean flow rate relative to each injection type, namely 80 L/h for mist nozzles and 220 L/h for the rest of the solutions. The rotation direction is varied so that the instrumented windings are artificially mirrored. For the three first injection tests, the location of winding 12 is maintained by swapping the rotation direction because windings 4 and 8 are interchanged. For windings 4 and 8, the expected inverse effects are observed on the whole. Differences mainly result from a very local phenomenon as only a stator tooth separates both locations. In the multi-jets case, the stator position enables a better representation of the winding temperature profile along the radial position. An approximate profile of the mean winding temperature is shown in Fig. 15.

Interestingly, a significant disparity can be perceived for all solutions. Indeed, as ΔT does not exceed 40 °C for these tests, the winding temperature differences in the whole domain may reach more than 30 °C for some measurements. Within the same winding, differences of 20 °C can be observed. It is necessary to highlight the importance of inner winding gradients. Analyses must be conducted bearing in mind that the temperatures must be compared by their positions (slot, yoke or tooth). Considering a reference temperature for each winding, the temperature disparity along the radial position may not be as important as it first appeared. In Fig. 15, the reference temperature corresponds to the average of the measured temperatures of a considered winding. Disregarding the inner winding gradients, the disparity in this case is reduced to approximately 8 °C. In comparison, dripping and mist nozzle disparities are approximately 9 and 11 °C, respectively.

Without rotation, the oil distribution seems to be much more uncertain because the temperature disparities are even more pronounced. This is a configuration somewhat apart for all injectors.

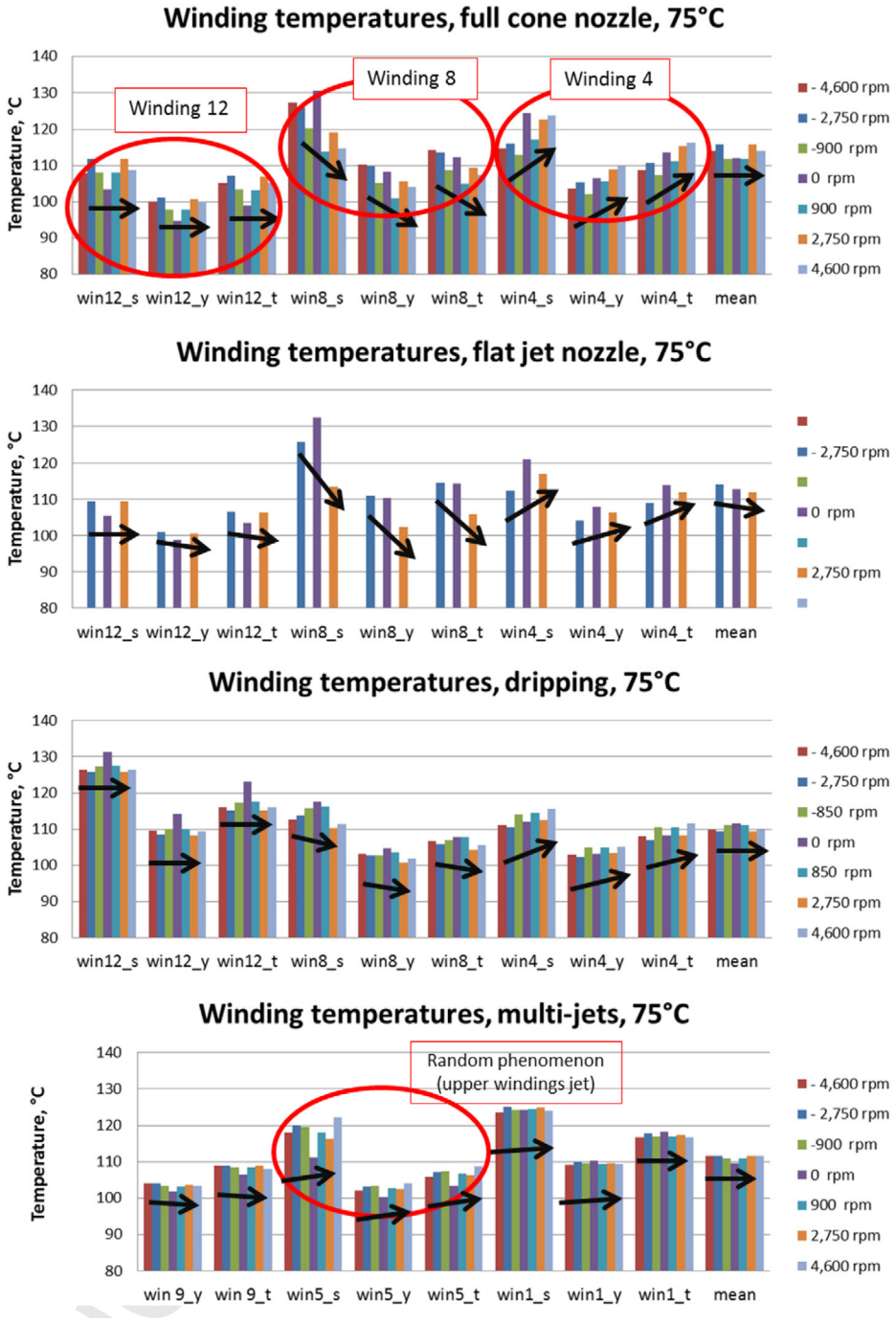

Fig. 14. Influence of the rotation speed on the winding core temperature (relative mean flow rate).

Local hotspots confirm the minimisation of the global cooling efficiency.

It must be noted that the upper winding is the coldest for the mist configuration, contrary to the dripping and multi-jets configurations for which upper windings are the warmest. In the former case, this can be explained by the vicinity of the upper winding to the impinging zone. Although impingement is not directed on windings, the upper winding benefits from concentrated oil at a high velocity. In the latter case, the upper windings only benefit from the low velocity injected oil, while convection on the lower windings is improved. The various projections observed in the lower region might have some influence on this finding.

Oil cooling is observed to be significantly affected by gravity effects. Rotation also influences the temperature field. However, this influence varies for the different configurations. For mist nozzles, the impact is important as the winding temperature can differ by 10 °C between $-\omega^{max}$ and $+\omega^{max}$, considering each winding temperature. The impact is less pronounced for dripping as maximum differences approach 5 °C. Concerning the multi-jets injector, the influence is roughly negligible, except for the lower windings where the jets from the upper windings randomly impact. These unsteady effects have been detected during measurement; unstable data are noted in the bottom graph of Fig. 14 (winding 5).

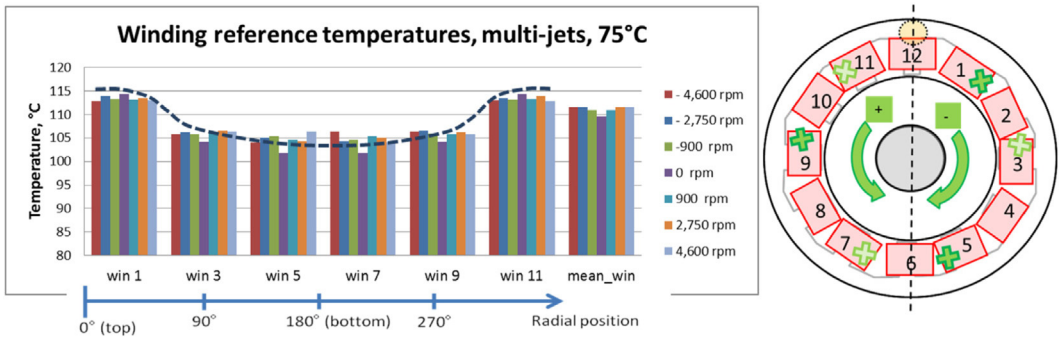

Fig. 15. Winding reference temperature profile along the radial position for the multi-jets configuration (220 L/h oil flow rate).

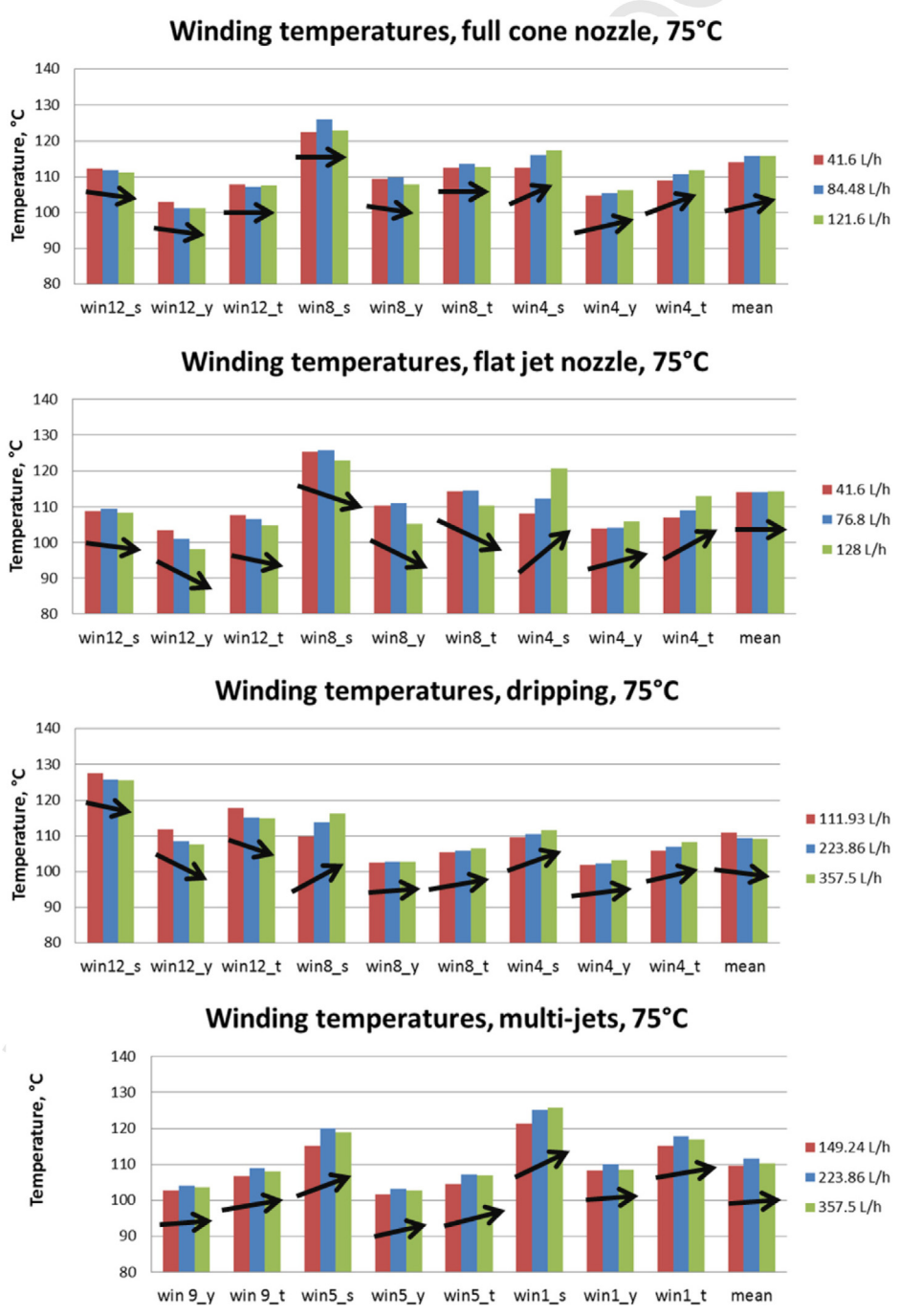

Fig. 16. Influence of the oil flow rate on winding core temperature (rotor speed = −2750 rpm).

DOI : 10.1016/j.applthermaleng.2014.10.060

The temperature measurements are consistent with the visualisation. The concentration of oil in the lower-right quadrant for a clockwise rotation corresponds to a lower winding temperature. Mist generators are the most influenced by the rotation, globally and locally. Most likely, the global trend for reduced heat transfer with rotation speed is due to the resulting disparities. The impact is smaller for the dripping configuration but can be locally observed.

2.6.2. Impact of oil flow on local temperatures

The impact of oil flow studied next. The rotation speed employed for comparison is set to 2750 rpm. For all configurations, the entire relative flow rate range is represented (Fig. 16).

For both nozzles, the greater the flow rate, the more efficient is the cooling for upper windings (see winding 12) that are close to the impingement zone. However, differences due to rotation in the lower part seem to decrease with increasing flow rate. It is observed in the top of Fig. 16 that at the lowest rate, winding 8 is significantly warmer than winding 4. The two winding temperatures converge as the flow rate is augmented.

In the dripping case, with an increase of flow rate, an important temperature homogenisation is perceived. Indeed, both bottom windings, which turn out to be better cooled for dripping, approach the mean temperature for a rising flow rate. The upper winding remains the hot spot in spite of oil spilling directly onto it. When the flow is of more importance, its cooling is improved, but not substantially more than the global trend. This might be explained by the low output oil velocity even at the maximum rate. The influence of flow rate in the multi-jets case is not clear as the instrumented winding temperatures seem to increase slightly more than the mean trend.

3. Conclusions

In this study, different oil cooling injections have been investigated. The presence of oil, even a restricted amount, significantly improves global heat transfer compared to air only. Indeed, with oil injection, the dissipation power is multiplied by a factor 2.5 to 5. Both mist pattern injectors tested led to similar conclusions. The cooling efficiency of these nozzles is close to those of the two other injection types in spite of a lower flow rate. The dripping injector is the most efficient, as oil is injected at the top region, and the end-winding surfaces benefit from a higher flow rate. Jet impacts remain local and appear to be ineffective.

For all configurations, the oil flow rate is the main factor for global efficiency. An increase in the oil flow rate always improves winding cooling. Contrary to reference case without oil, an increase in the rotation speed does not enhance the global efficiency. That might be explained by the local approach.

Local measurements complemented by flow pattern observations highlight important temperature disparities, mostly caused by gravity effects. In the mist nozzle and dripping cases, the concentration of drops and droplets is dense, and a substantial part of the flow rate is directed toward the rotating parts, thus redistributing oil within the domain. The rotation speed therefore affects the local temperature. For these systems, increasing the rotor speed results in augmenting the disparities while increasing the flow rate generally leads to decreased disparities. For multi-jets, the oil distribution is not clearly influenced by the two parameters. Because local temperature measurements on the windings were restricted, the local approach may not reflect some effects.

Further work is needed to quantify the oil convection coefficients to model the thermal behaviour of an actual machine. This identification will be performed using an inverse method. Viscosity effects might appear more clearly with this approach as the dissipation powers are related to the temperature difference between the oil and the winding surface.

References

[1] Y. Bertin, Refroidissement des machines électriques tournantes, Tech. Ing. (1999) D3460.
[2] Y. Bertin, Refroidissement des machines tournantes. Études paramétriques, Tech. Ing. (2006) D3462.
[3] D. Staton, A. Boglietti, A. Cavagnino, Solving the more difficult aspects of electric motor thermal analysis in small and medium size industrial induction motors, IEEE Trans. Energy Convers. 20 (2005) 620–628.
[4] D.-A. Staton, M. Popescu, D. Hawkins, A. Boglietti, Influence of different end region cooling arrangements on end-winding heat transfer coefficients in electrical machines, Energy Convers. Congr. Expo. (ECCE) (2010) 1298–1305.
[5] N. Hay, D. Lampard, S. Pickering, T.-F. Roylance, Heat transfer from the stator end-windings of a low-voltage lap-wound electric motor, in: Seventh International Conference on Electrical Machines and Drives, 1995, p. 412.
[6] M. Pais, L. Chow, Jet impingement cooling in VSCF generators, in: SAE, Aerospace Atlantic Conference, Dayton, Ohio, 1995.
[7] C. Ma, Q. Zheng, Local heat transfer and recovery factor with impinging free-surface circular jets of transformer oil, Int. J. Heat Mass Transfer 40 (1997) 4295–4308.
[8] D. Zhou, C. Ma, Radial heat transfer behavior of impinging submerged circular jets, Int. J. Heat Mass Transfer 49 (2006) 1719–1722.
[9] H. Sun, C. Ma, Y. Chen, Prandtl number dependence of impingement heat transfer with circular free-surface liquid jets, Int. J. Heat Mass Transfer 41 (1998) 1360–1363 n° 10.
[10] D. Wadsworth, I. Mudawar, Enhancement of single-phase heat transfer and critical heat flux from an ultra-high-flux simulated microelectronic heat source to a rectangular impinging jet of dielectric liquid, J. Heat Transfer 114 (1992) 764–768.
[11] D. Womac, G. Aharoni, F. Incropera, Correlating equations for impingement cooling of small heat sources with single circular liquid jets, J. Heat Transfer 116 (1993) 106–115.
[12] J. Kim, Spray cooling heat transfer: the state of the art, Int. J. Heat Fluid Flow 28 (2007) 753–767.
[13] B. Abbasi, J. Kim, A. Marshall, Dynamic pressure based prediction of spray cooling heat transfer coefficients, Int. J. Multiph. Flow 36 (2010) 491–502.
[14] E.A. Silk, J. Kim, K. Kiger, Spray cooling of enhanced surfaces: impact of structured surface geometry and spray axis inclination, Int. J. Heat Mass Transfer 49 (2006) 4910–4920.
[15] K. Oliphant, B. Webb, M. McQuay, An experimental comparison of liquid jet array and spray impingement cooling in the non-boiling regime, Exp. Therm. Fluid Sci. 18 (1998) 1–10.
[16] N. Karwa, S. Kale, P. Subbarao, Experimental study of non-boiling heat transfer from a horizontal surface by water sprays, Exp. Therm. Fluid Sci. 32 (2007) 571–579.
[17] F. Kreith, Convection heat transfer in rotating systems, Adv. Heat Transfer, in: Irvine, Hartnett (Ed.), vol. 21, 1968.
[18] J. Owen, M. Rogers, Flow and heat transfer in rotating disk systems, Rotor Stator Syst. e1 (1989).